Cellulose (2019) 26:5571–5582
https://doi.org/10.1007/s10570-019-02482-1

ORIGINAL RESEARCH

One-step fabrication of imprinted mesoporous cellulose nanocrystals films for selective separation and recovery of Nd(III)

Xudong Zheng · Yi Zhang · Tingting Bian · Dandan Wang · Zhongyu Li

Received: 13 February 2019 / Accepted: 6 May 2019 / Published online: 11 May 2019

Abstract Previously, we investigated imprinted silica films templated by cellulose nanocrystals for the selective adsorption of rare earth ions from acidic systems, but the cost of organosilane limits the application of silica film adsorbents. Considering the cost and outstanding properties of cellulose, converting this renewable biological resource into an adsorbent material is a vital step towards sustainable development. One-step fabrication of imprinted mesoporous cellulose nanocrystals films (IMCFs) was implemented via ionic imprinting technology and they were applied to efficiently and selectively separate neodymium ions [Nd(III)]. Transmission photographs clearly demonstrated there is a highly ordered mesoporous structure after removal of silicon source. Nitrogen adsorption measurements showed two obtained materials possess high specific surface area, providing a good premise for efficient separation. When employed as absorbents, the maximum adsorption capacity of IMCFs is almost three folds than that of NIMCFs, reaching 18.22 mg g^{-1}. The distribution coefficient of IMCFs for Nd(III) reached 435.46 mL g^{-1}, much higher than other interfering ions. Repeatability tests showed IMCFs retained 81.55% of initial adsorption capacity after five adsorption cycles. In summary, this work presents a new avenue to construct imprinted mesoporous cellulose nanocrystals films for separation of rare earth ions.

Keywords Neodymium · Ionic imprinted polymers · Cellulose nanocrystals films · Selective separation · Rare earth

Electronic supplementary material The online version of this article (https://doi.org/10.1007/s10570-019-02482-1) contains supplementary material, which is available to authorized users.

X. Zheng (✉) · Y. Zhang · T. Bian · D. Wang · Z. Li (✉)
School of Environmental and Safety Engineering, Changzhou University, Changzhou 213164, People's Republic of China
e-mail: zhengks@outlook.com

Z. Li
e-mail: zhongyuli@mail.tsinghua.edu.cn

Z. Li
Jiangsu Key Laboratory of Advanced Catalytic Materials and Technology, School of Petrochemical Engineering, Changzhou University, Changzhou 213164, People's Republic of China

Introduction

Neodymium (Nd), one of the critically rare earth elements (REEs), is widely employed in neodymium-iron-boron (NdFeB) magnets, where the Nd content is as high as 26% (Chen et al. 2015; Sprecher et al. 2014). The surge in magnet consumption has produced

amounts of rare earth wastes (such as end-of-life NdFeB magnets). The long-term unreasonable disposal and utilization of these wastes has created serious environmental issues and posed serious threats to human health and ecosystems (Johannesson et al. 2017; Zhao et al. 2017; Du et al. 2018). Hence, with rapid increase of the demand for Nd in magnets and consideration of environmental factors, the recycling of Nd has become a significant issue (Moriwaki et al. 2016; Won et al. 2015).

Conventional methods employed for REEs extraction in industrial applications include pyrometallurgical and hydrometallurgical processes (Yoon et al. 2015). Pyrometallurgical methods utilize high temperature heating to peel off nonmetallic materials, allowing valuable metals to be melted into other metal melts or molten salts (Fröhlich et al. 2017). By increasing reaction temperature and prolonging reaction time, Bian extracted Nd_2O_3 from waste NdFeB permanent magnet scraps with the purity of 95% (Bian et al. 2015). Although REEs can be separated effectively in this way, but inevitably require abundant of energy injection. Hydrometallurgy based on different affinities of REEs is considered to be a flexible, high selective and environmentally friendly strategy (Royen and Fortkamp 2016). Extraction of target metals from leachate via solvent extraction, precipitation, displacement, ion exchange, and electrolytic extraction (Swain 2017; Tunsu et al. 2016). Among of them, emerging solid–liquid extraction (SLE) strategy is a greener alternative, in which does not require large volumes of organic solvent and provide better separation factors (eFlorek et al. 2014; Moloney et al. 2014; Sun et al. 2013). For SLE strategy, the most critical thing is to study and prepare novel adsorption materials.

Currently, nanomaterials with special morphology and well-designed porous structures are the focus and hotspot, while lacking of specific recognition, high cost, and difficulty in subsequent separation remain key issues restricting their large-scale application. Macroscopical assembly of nanomaterials is the key to practicability of nanomaterials. Among them, self-assembly has received extensive attention due to no need of external intervention and precise assembly (Service 2005). Rod-like cellulose nanocrystals (CNCs, typically 3–10 nm in width, 100–500 nm in length) are obtained by sulfuric acid-catalyzed hydrolysis from bulk cellulose (Yao et al. 2017). CNCs feature an attractive combination of excellent mechanical and thermal properties, high Young's modulus, high crystal structure, high aspect ratio and large surface area, making them become ideal polymer matrices for nanocomposite construction (Li et al. 2018). Abundant hydroxyl groups on the surface of CNCs show negative charges and they are easily chemically modified, which enhance their dispersibility in hydrophobic matrix materials and expand the range of applications (Dufresne 2017; Voisin et al. 2017). When subjected to solvent evaporation induced self-assembly (EISA), CNCs have the ability of self-assembly into a chiral nematic (cholesteric) liquid crystal films with a helical arrangement (Lagerwall et al. 2014). Benefited from its intriguing behavior, many studies reported CNCs were used as a soft template to construct organic–inorganic hybrid films by adding small molecular tetraethoxysilane (TEOS), tetramethoxysilane (TMOS) and tetrabutyl titanate (TBT) as precursors. After removal of CNCs through calcination or acid treatment, films with highly ordered, mesoporous, iridescent color can be obtained. These films have been proven to have good adsorption properties for metals and metalloid ions in aqueous solutions (Gao and Jin 2018; Terpstra et al. 2018; Xue et al. 2017).

Moreover, adsorption of high purity single rare earth element from a mixed system is difficult due to their chemical similarity (Xie et al. 2014). Ionic imprinting technology (IIT) has attracted widespread attention because of its recognition of target ions, predictability of structure, specificity of recognition and universality of applications (Fu et al. 2015; Wang et al. 2017; Pan et al. 2018; Wei et al. 2018). Through specific coordination or electrostatic interactions, ionic imprinted polymers (IIPs) repolymerized by template and functional monomers are generally compatible with aqueous media (Dai et al. 2018). After eluting metal ions, imprinting sites matching the spatial configuration of imprinted ions were left. These stable imprinted sites will help to effectively increase adsorption capacity of films.

Combining macroscopical assembly of nanomaterials and ionic imprinting technology, imprinting sites may enter the mesoporous wall and surface to a greater extent, making it more conducive to capturing target ions. Patra proposed a novel coating adsorbent based on Gd(III)-ordered magnetic mesoporous carbon (OMMC) and filled in a small sized micropipette tip

of a micropipette for microsolid phase detection (Patra et al. 2017). Liu employed mesoporous Fe_3O_4@PEI-SBA-15 as template and endowed vinyl groups by surface modification. Finally, Sr(II)-imprinted polymer was successfully synthesized with the help of AIBN as initiator (Liu et al. 2015). Our previous study reported a novel strategy of silica composite films templated by CNCs prepared via dual-template docking oriented ionic imprinting (Zheng et al. 2017, 2018). CNCs interacted with Nd(III) to form dual-template docking configuration. After remove of CNCs (structural orientation template) and Nd(III) (imprinting template), imprinting silica films exhibit high selective adsorption capacity for Nd(III). Nevertheless, there are still several distinct drawbacks: 1) after removal of templates, remaining silica films are less flexible and quite brittle; 2) it requires numerous chemical reagents and high cost of Si source precursors (like TEOS and GLYMO-IDA). This prompted us to work on the research of greener, low-cost and good flexibility imprinted mesoporous composite films. After our research, we found that CNCs can be directly used to prepare macroscopical assembly of nanomaterials with excellent properties. Surface groups of CNCs also provide the possibility for the formation of imprinted sites.

Our intention is to develop an environmentally friendly, low-cost imprinted mesoporous material for efficient and selective recovery Nd(III) from end-of-life NdFeB magnets. In this study, inspired by CNCs and IIT, we proposed one-step fabrication of imprinted mesoporous cellulose nanocrystals films (IMCFs). In contrast to our previous studies, at this time, CNCs as the function of membrane unit, tetraethoxysilane (TEOS) and Nd(III) existed as sacrificial templates and imprinted templates, respectively. CNCs/organosilica composite films were obtained via EISA method. Subsequently, silicon source and Nd(III) were removed by alkali treatment and weak acid elution, respectively. Corresponding reference NIMCFs, using the same procedure except adding Nd(III). The whole adsorption experiments were carried out under acidic conditions to simulate a real harsh adsorption environment, where NdFeB magnets were dissolved by strong acid. Before adsorption tests, we fully characterized the IMCFs and NIMCFs, such as surface interface morphology, pore properties, and crystal structure changes, to ensure the successful preparation of the materials. To reveal adsorption properties of IMCFs and NIMCFs on Nd(III), various operating parameters such as solution pH, contact time, and initial Nd(III) concentration on adsorption efficiency were systematically investigated. Experimental data were further studied by multiple mathematic models to confirm intrinsic adsorption mechanism. In addition, adsorption selectivity and reusability were also discussed in detail to predict the prospects and potential for industrial applications.

Experimental section

Materials

Tetraoxyethyl silane (TEOS) was purchased from Aladdin Chemicals Co., Ltd. Dextrose, ethanol, nitric acid (HNO_3), anhydrous hydrochloric acid (HCl, 37%) and rare earth oxides (4 N) were obtained from Sinopharm Chemical Reagent Co., Ltd. Medical absorbent cotton was purchased from Shanghai Yinjing Medical Sanitary Materials Co., Ltd. Experimental water is the double distilled water (DDW). All reagents do not need further purification.

Preparation of CNCs

According to our previous study (Zheng et al. 2018, 2019a, b). 10 g of cotton was hydrolyzed by sulfuric acid (64 wt%, 15 mL of sulfuric acid/g cotton) at 45 °C for 2 h. Subsequently, about tenfold of cold water was added to quench the reaction, and put overnight. The upper clear liquid was discarded and lower sediment was centrifuged. The obtained product was sonicated for 30 min at 600 W with an ultrasonic cell pulverizer. Finally, the mixture was poured into dialysis bags (Mw12000-14000 KD) and dialyzed for a week, until the pH of the suspension reached 2.4.

Preparation of imprinted mesoporous cellulose nanocrystals films

5 mg of glucose, 200 μL of TEOS, and 4 mg of neodymium nitrate were dissolved in 10 mL of above CNCs suspension. After stirring at 60 °C for 2 h, the white homogeneous slurry was poured into polytetrafluoroethylene disk and dried at room temperature, slowly evaporated and then got complete films, that is, CNCs/organosilica composite films. Subsequently,

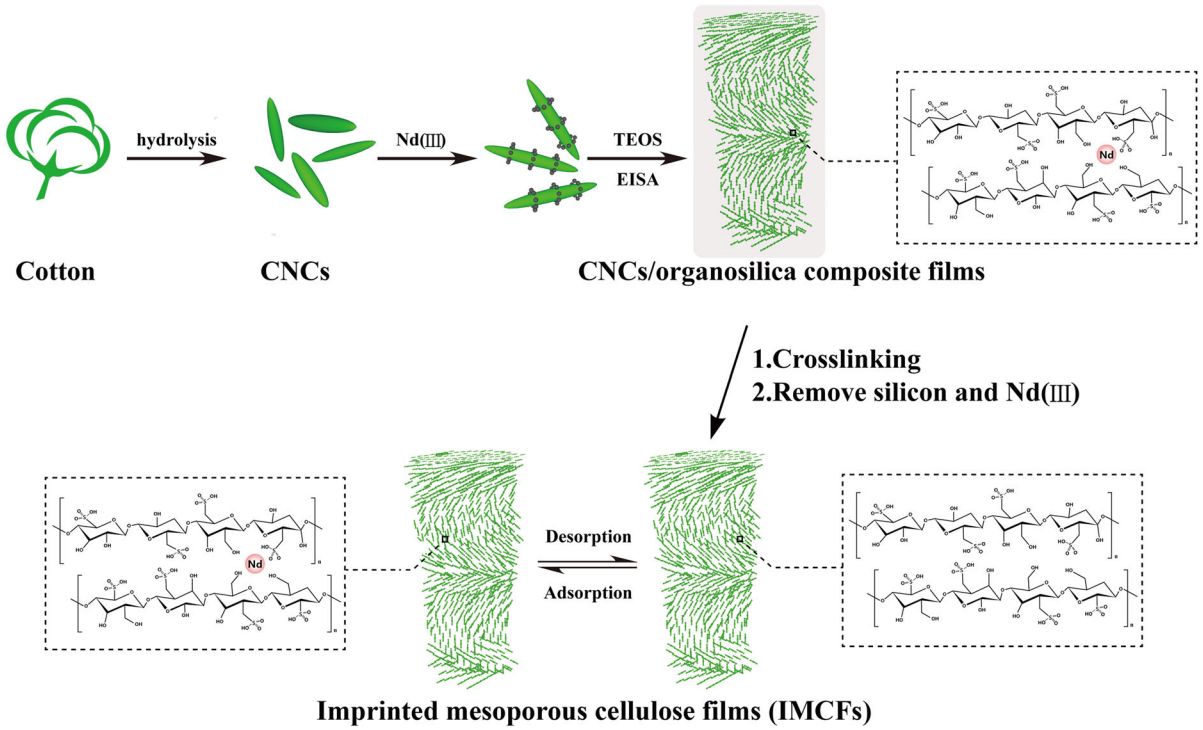

Scheme 1 Schematic diagram of the free-standing imprinted mesoporous cellulose films (IMCFs)

these films were placed in 1.83 M NaOH solution (1 mL of sodium hydroxide per 10 mg film), repeated several times to ensure Si materials have been completely removed. After that, eluate was prepared by 1:9 (v/v) glacial acetic acid and DDW. Above films were immersed in the eluent and oscillated in water bath to remove Nd(III). Finally, films were cleaned 2–3 times with DDW, and left to dry under ambient temperature. At this point, desired materials IMCFs have been successfully prepared. Non-imprinted mesoporous cellulose films (NIMCFs) also follow the above preparation process, expect the addition of Nd(III). Hence, there is no need to conduct acid treatment. Scheme 1 describes the synthesis process of IMCFs.

Results and discussion

Morphology analysis

Morphology of IMCFs were observed by SEM and TEM. From the macroscopic level, as shown in Fig. 1, the film can achieve 90° bending, exhibiting good flexibility and definite mechanical properties. It is mainly because cellulose and the moisturizing effect of glucose makes film flexible. Figure 2 displays pictures of cross-sectional IMCFs and NIMCFs which were characterized by SEM and TEM. It can be observed that both IMCFs and NIMCFs exhibit highly ordered liquid crystal nematic structure (Fig. 2a, b), which benefits from intrinsic nano-structure of CNCs, indicating films have been prepared successfully. To further confirm whether the silicone has been completely removed, IMCFs and NIMCFs were scanned by energy dispersive X-ray spectroscopy (EDS). As shown in Fig. S1, films mainly contain C/O, moreover, the content of Si is basically negligible, proving that silicon source has been removed completely during alkali treatment. TEM further confirms the pore morphology (Fig. 2c, d). Cellulose could not bear high temperature. When electrons hit on the surface of films, a certain degree of melting occurs, making photos appear slightly blurry. TEM shows IMCFs display uniformly arranged pore structure. More importantly, elution process does not result in the

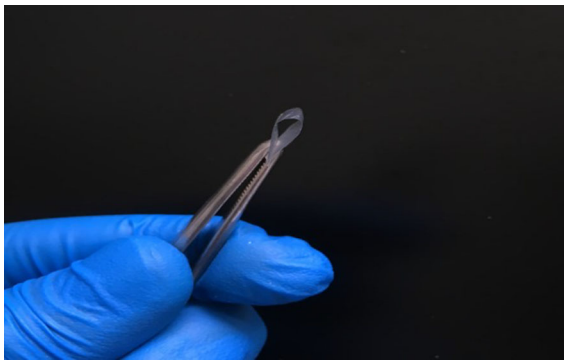

Fig. 1 Flexibility display of IMCFs

destruction of chiral liquid crystal structure of CNCs. All this confirm the successful preparation of IMCFs and NIMCFs.

Specific surface area, pore volume and pore size distribution of IMCFs and NIMCFs were measured by nitrogen adsorption and desorption isotherms. Figure 3 shows isotherm type corresponds to type IV with an H1 hysteresis loop, associated with mesoporous nanocellulose. Table 1 lists corresponding parameters of IMCFs and NIMCFs. IMCFs illustrates a BET surface area of 56.82 m^2 g^{-1}, a BJH adsorption cumulative pore volume of 0.03071 cm^3 g^{-1}, and a BJH adsorption average pore width of 2.1790 nm, compared 53.06 m^2 g^{-1}, 0.02825 cm^3 g^{-1}, 2.0499 nm of NIMCFs. In the process of alkali treatment, the BET surface area of films may decrease to a certain extent. By virtue of flexibility, mesoporosity and highly ordered structure give potential applications for separation of REEs.

Surface characterization

Fourier transform infrared (FT-IR) analysis attempted to characterize the surface groups of IMCFs and NIMCFs. Fig. S2 shows there is no significant difference between IMCFs and NIMCFs in terms of

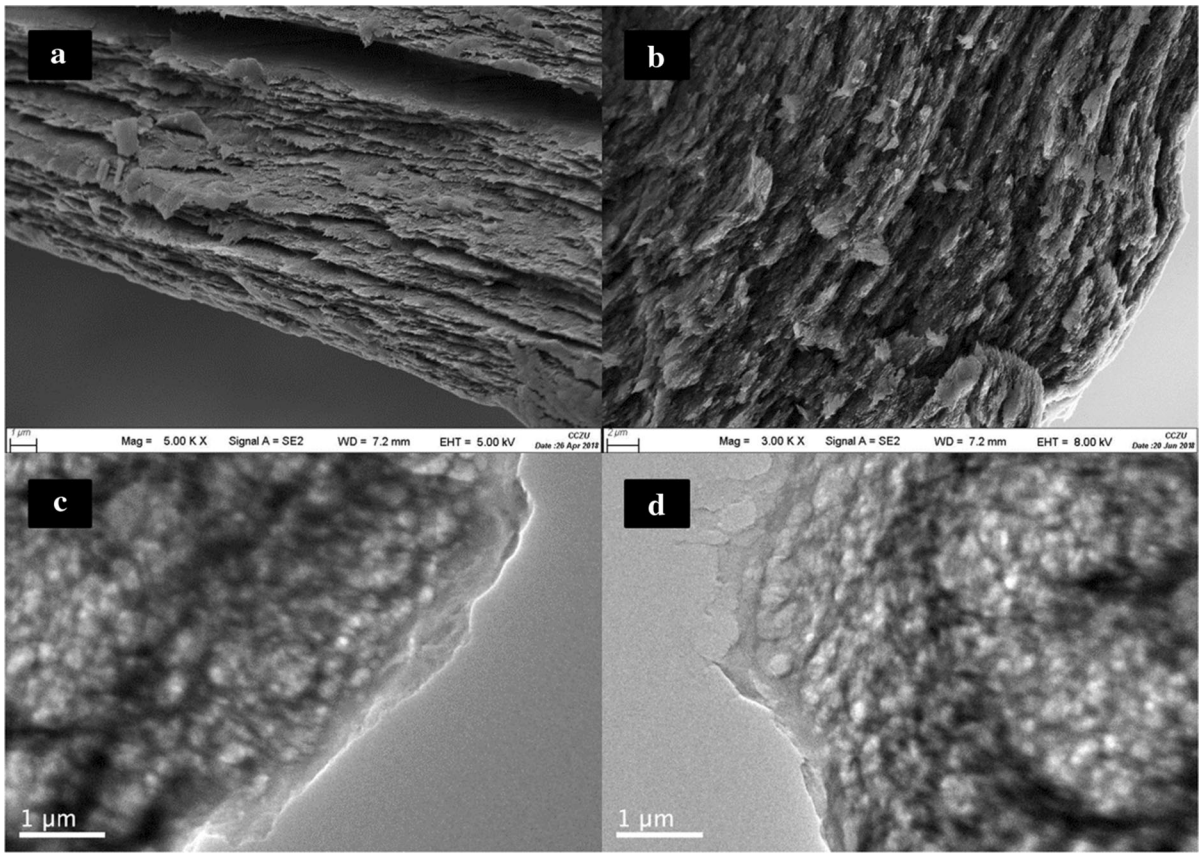

Fig. 2 SEM images of **a** IMCFs, **b** NIMCFs and TEM images of **c** IMCFs, **d** NIMCFs

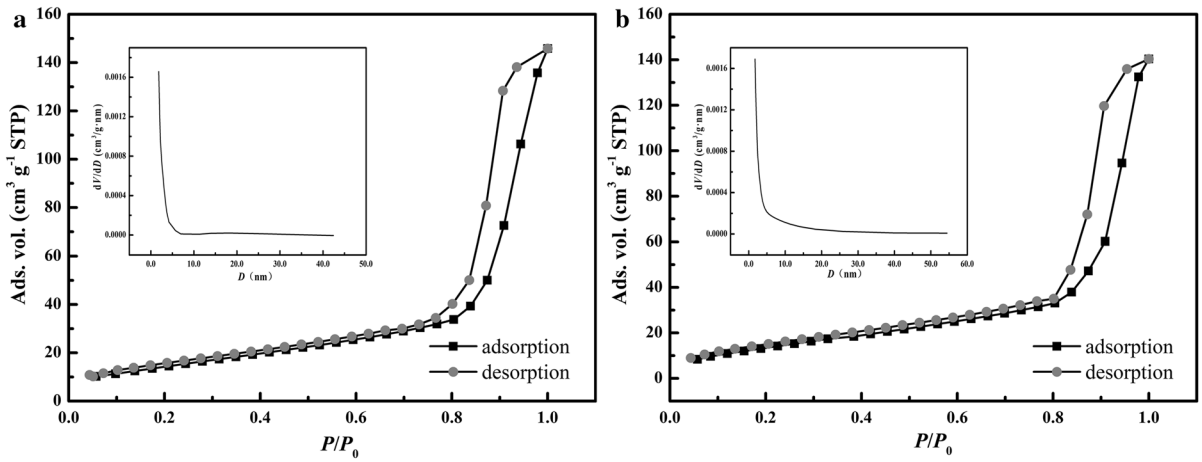

Fig. 3 N_2 adsorption–desorption isotherms and pore size distributions (insert) for IMCFs (**a**) and NIMCFs (**b**)

Table 1 Brunauer–Emmet–Teller surface areas (S_{BET}) obtained by N_2 adsorption–desorption measurements for IMCFs and NIMCFs

Materials	S_{BET} (m^2 g^{-1})	Pore size (nm)	V_{proe} (cm^3 g^{-1})
IMCFs	56.82	2.1790	0.03071
NIMCFs	53.06	2.0499	0.02825

FT-IR spectra. Cellulose characteristic peaks at 3650–3200 cm^{-1} (the stretching of intra- and intermolecular O–H and –CH_2OH vibrations), 2902 cm^{-1} (asymmetric C–H stretching vibration), 1337 cm^{-1} (C–O–H bending) and 1160 cm^{-1} (C–O–C stretching motion) are present in both IMCFs and NIMCFs. Overall, all this confirmed CNCs structure has been preserved and further verified the successful preparation of IMCFs and NIMCFs.

Crystal properties of IMCFs and NIMCFs, and IMCFs after five adsorption cycles were evaluated by X-ray diffraction, as displayed in Fig. S3. Calculated by jade 6 software, characteristic peaks at 2θ = 14.7°, 16.8°, 22.7°, and 34.7°, assigning to the (1–10), (110), (200) and (004) crystal planes, respectively, where diffraction characteristics are similar to typical semicrystalline cellulose type I. From the figure, it can be inferred that CNCs have high crystallinity and their crystal form can be preserved after five adsorption cycles. Compared with IMCFs, the crystallinity of IMCFs after repeatability experiments has a significant loss, which may attribute to destruction of the crystallinity of cellulose by acid elution.

Thermogravimetric analysis (TGA) outline the thermal stability and composition of IMCFs and NIMCFs under nitrogen atmosphere. Fig. S4 shows the variation in total weight with temperature. The weight loss of two materials are about 74.02% (IMCFs) and 75.55% (NIMCFs), respectively. Within the initial temperature range (0–150 °C), IMCFs decreased significantly by about 10%, mainly due to the loss of residual water. IMCFs are proved as hydrophilic materials, which will take advantages of the recovery of REEs in solid–liquid extraction separation. It is obvious that the loss of total weight of IMCFs is gentler than that of NIMCFs, indicating better thermal stability. Moreover, the total weight loss of IMCFs was about 54.58% at 200–300 °C, corresponding to the thermal decomposition of nanocellulose.

Effect of pH

pH value plays a decisive role in the adsorption process, which affects the protonation of the adsorbent surface and the ionization degree of adsorbates. The recovery of REEs generally occurs under acidic condition. When pH > 7.0, REEs will produce hydroxide precipitation. Hence, pH tests were conducted between 2.0 and 7.0. Adsorption capacities [Q_t (mg g^{-1})] were obtained by Eq. (1):

$$Q_t = \frac{V(C_0 - C_e)}{m} \quad (1)$$

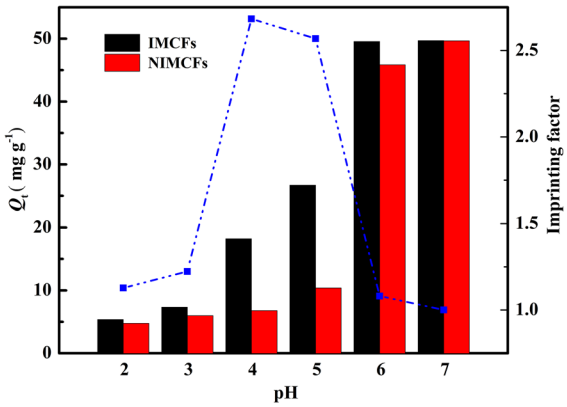

Fig. 4 The effect of pH on the adsorption capacity of IMCFs and NIMCFs

where C_0 and C_e (mg L^{-1}) represent initial and residual concentration of Nd(III) in solution. V (10 mL) denotes the volume of stock solutions while m (10 mg) stands for the mass of adsorbent.

As seen in Fig. 4, as pH value increases, the adsorption efficiency and capacity of IMCFs and NIMCFs showed different degrees of increase, demonstrating higher pH is helpful for the absorption. At lower pH, Q_t of IMCFs is significantly superior to NIMCFs, attributed to the lack of imprinting sites of NIMCFs. When pH value was 7.0, Q_t of imprinted films and non-imprinted films reached 49.70 and 49.66 mg g^{-1} (concentration of the stock solution is 50 mg L^{-1}), which means acidic solution system does affect the adsorption properties of two materials indeed. Zeta potential of pH on IMCFs and NIMCFs are displayed in Fig. S5. When pH value is 4.0, the Zeta potential of IMCFs is − 4.944 mV, whereas that of NIMCFs is − 0.15 mV. It illustrates the pH range of surface protonation, owing to the imprinting effect, IMCFs provide highly selective space sites under acidic condition. Hence, IMCFs exhibited high adsorption capacity. Generally, rare earth ions can be dissolved by strong acids, so it makes more sense to adsorb Nd(III) under acidic condition. The acidic hydrolysis of CNCs results in the existence of residual acid groups on its surface, so these films will be more favorable for separation and recovery of Nd(III) under acidic condition. The imprinting effect of adsorbents is measured by imprinting factor (IF), which can be calculated from the ratio of the adsorption amount of IMCFs and NIMCFs. pH ranges from 2.0 to 7.0 were employed to test the impact under extreme conditions. Although the adsorption capacity is much lower than that of pH = 7.0, the maximum value of IF is 2.68 at pH = 4.0. At this point, the distinction between IMCFs and NIMCFs is the most obvious, and the effect of imprinting sites on adsorption performance is also the most significant. Therefore, by considering above factors, the initial stage pH of solution was determined as 4.0.

Kinetics

The variation of Q_t with adsorption time onto IMCFs and NIMCFs were described in Fig. 5. Before reaching the adsorption equilibrium, both IMCFs and NIMCFs have undergone a rapid adsorption process within the first 200 min of contact, then adsorption rate decreased, which may be caused by the absence of the imprinted sites immobilized on films. The equilibrium adsorption capacity of IMCFs is 18.22 mg g^{-1}, significantly higher than that of NIMCFs (6.79 mg g^{-1}), indicating IMCFs show better affinity toward Nd(III). Pseudo-first-order kinetic model [PFOKM, Eq. (2)] and pseudo-second-order kinetic model [PSOKM, Eq. (3)] were calculated to elucidate the adsorption rate and rate-limiting steps.

$$Q_t = Q_e - Q_e e^{-k_1 t} \tag{2}$$

$$Q_t = \frac{k_2 Q_e^2 t}{1 + k_2 Q_e t} \tag{3}$$

where k_1 (min^{-1}) and k_2 (g mg^{-1} min^{-1}) are the adsorption rate constant of PFOKM and PSOKM, respectively. Further, in pseudo-second-order dynamics equation, h (g mg^{-1} min^{-1}) represents initial sorption rate, i.e. initial adsorption rate when t approaches to zero [Eq. (4)]. $t_{1/2}$ stands for half-balanced time [Eq. (5)]:

$$h = k_2 Q_e^2 \tag{4}$$

$$t_{1/2} = \frac{1}{k_2 Q_e} \tag{5}$$

Table 2 summaries kinetic parameters and correlation coefficients. PSOKM fits two adsorbents with higher correlation coefficients (R^2): 0.997 of IMCFs and 0.998 of NIMCFs, a basic assumption that the adsorption process belongs to chemical adsorption. The equilibrium adsorption capacity of IMCFs and

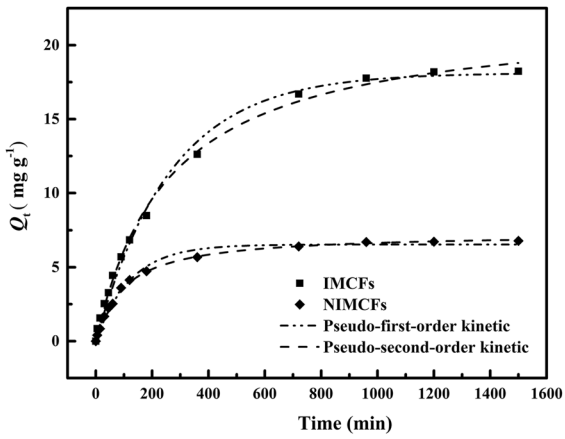

Fig. 5 Kinetic data and modeling for the adsorption of Nd(III) on IMCFs and NIMCFs, Error bar represents the standard deviation of kinetic data (pH = 4.0, 298 K, 50 mg L^{-1})

NIMCFs predicted by PSOKM is 22.05 mg g^{-1} and 7.31 mg g^{-1}, respectively. Kinetic tests indicate active sites on IMCFs show a good affinity to Nd(III).

Adsorption isotherms

To investigate adsorption performance of IMCFs and NIMCFs on Nd(III), adsorption isotherms were measured by contacting adsorbents with different concentrations of Nd(III) stock solution. The adsorption capacity reached maximum when initial concentration is 150 mg L^{-1}, once all active sites were occupied, the adsorption reached equilibrium. In order to describe and understand the adsorption mechanism, two isotherm models, Langmuir [Eq. (6)] and Freundlich [Eq. (7)] models (Langmuir 1916), were employed to fit adsorption data. Two relationships are listed as below:

$$Q_e = \frac{K_L Q_m C_e}{1 + K_L C_e} \quad (6)$$

$$Q_e = K_F C_e^{1/n} \quad (7)$$

where C_e (mg L^{-1}) represents the concentration of solution at equilibrium. Q_m (mg g^{-1}) is the maximum Nd(III) uptake. K_L (L mg^{-1}) is the Langmuir constant denoted the energy of adsorption and affinity of binding sites. n and K_F (mg g^{-1}) are both Freundlich constants, indicating the adsorption strength and capacity, respectively.

Fittings of adsorption isotherms are displayed in Fig. 6. Isotherm constants and correlation coefficients obtained by adsorption equilibrium models are summarized in Table 3. Comparing with the Freundlich equation, results reveal Langmuir equations are fitted to experimental data for both of adsorbents sufficiently and show larger correlation coefficients (R^2) of 0.997 (IMCFs) and 0.996 (NIMCFs). Langmuir isotherm fits adsorption of Nd(III) better, which suggests it is a monolayer sorption. The maximum adsorption capacities of IMCFs and NIMCFs fitted by the equation are 23.03 mg g^{-1} and 9.31 mg g^{-1} (Table 3), which are close to the experimental data.

Selectivity test

Selectivity adsorption tests could detect whether IMCFs and NIMCFs have significant selectivity to Nd(III). Several rare earth cations [Dy(III), Gd(III), La(III), Tb(III)] with Nd(III) were added in coexistence system. The concentration of rare earth ions is the same (50 mg L^{-1}). Results were calculated by distribution coefficient K_d (mL g^{-1}), selectivity coefficient k and relative selectivity coefficient k'. Relationships are listed as follows [Eqs. (8), (9), (10)]:

Table 2 Kinetic constants for the Pseudo-first-order and Pseudo-second-order models

Materials	$Q_{e,exp}$ (mg g^{-1})	Pseudo-first-order kinetic model			Pseudo-second-order kinetic model				
		$Q_{e,c}$ (mg g^{-1})	K_1 (min^{-1})	R^2	$Q_{e,c}$(mg g^{-1})	$K_2 \times 10^{-2}$(g mg^{-1}min^{-1})	H (mg g^{-1}min^{-1})	$t_{1/2}$ (min)	R^2
IMCFs	18.22	18.12	0.0038	0.995	22.05	0.0175	0.0849	259.74	0.997
NIMCFs	6.79	6.535	0.0082	0.991	7.31	0.137	0.073	99.90	0.998

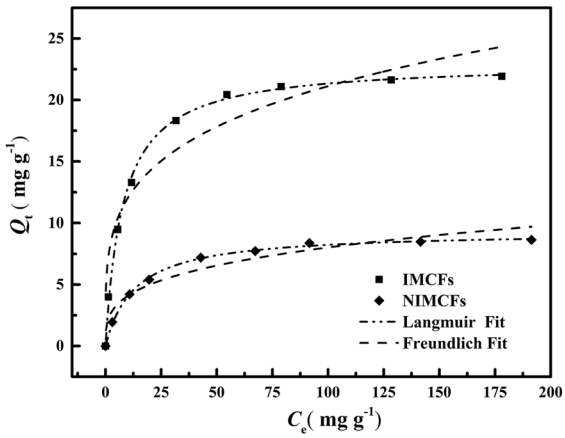

Fig. 6 Equilibrium data and modeling for the adsorption of Nd(III) on IMCFs and NIMCFs, Error bar represents the standard deviation of kinetic data (pH = 4.0, 298 K)

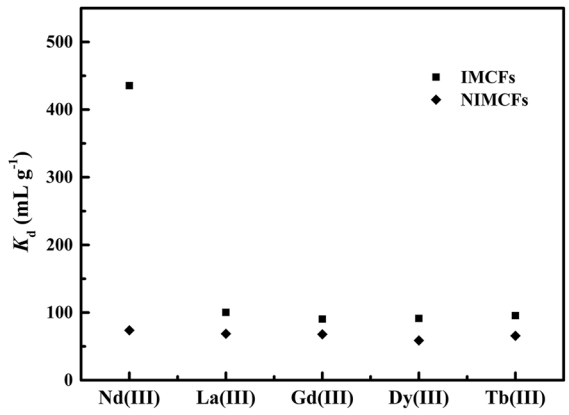

Fig. 7 K_d values of the IMCFs and NIMCFs for a mixture of Nd(III), La (III), Gd(III), Dy(III), and Tb(III), Error bars represent the standard derivation (pH = 4.0, 298 K, 50 mg L^{-1} for each ion)

$$K_d = \frac{V(C_0 - C_f)}{mC_f} \quad (8)$$

$$k = \frac{K_{d,1}}{K_{d,Nd(III)}} \quad (9)$$

$$k' = \frac{k_{(IMCFs)}}{k_{(NIMCFs)}} \quad (10)$$

where, C_0 and C_f are initial and residual concentration of each cation in batch system, respectively. The adsorption effect of imprinted films and non-imprinted films is presented in Fig. 7. Related data are summarized in Table 4.

From the figure, it can be concluded that K_d value (435.46 mL g^{-1}) of IMCFs toward Nd(III) is significantly higher over other cations, demonstrating IMCFs have a preferential affinity for Nd(III). This allows imprinted CNCs films to separate and adsorption of Nd(III) under interference ions. On the basis of Hard and Soft Acids and Bases (HSAB), residual acid groups (e.g., –SO_3H, –OH) on CNCs belong to hard base, while Nd(III) is typical hard acid. Hence, these groups react faster and form stronger bonds with Nd(III). In addition to special sites provided by IIT, which are only matched with Nd(III) on size. So, IMCFs show strong selective adsorption and separation ability during SLE. In order to further evaluate the performance of IMCFs, similar adsorbents are summarized and compared. From the Table 5, it can see that our materials have excellent adsorption capacity. Also, their advantages including safe, efficient, one-step reaction, and non-toxicity, which may provide an alternative method for recycling REEs (Dolak et al. 2015; Krishna et al. 2005; Melnyk et al. 2012; Vlachou et al. 2009; Zheng et al. 2016, 2017).

Reusability tests

Five cycles of binding and elution were used to test the reusability of IMCFs, which is of great significance for industrial applications. After each adsorption process, IMCFs were rinsed by elution and DDW, in order to remove the loaded Nd(III) completely. Figure 8 shows the variation of adsorption capacity at each binding-elution cycle. After five adsorption cycles, the

Table 3 Adsorption equilibrium constants for Langmuir and Freundlich isotherm equations

Sorbents	Langmuir isotherm equation				Freundlich isotherm equation		
	Q_m (mg g^{-1})	K_L (L mg^{-1})	R_L	R^2	K_F (mg g^{-1})	1/n	R^2
IMCFs	23.03	0.126	0.038	0.997	6.837	0.245	0.901
NIMCFs	9.31	0.076	0.0617	0.996	2.081	0.293	0.906

Table 4 K_d, k and k' values of Nd(III), Dy(III), Gd(III), La (III) and Tb(III)

Cation	IMCFs			NIMCFs			K'
	C_f (mg L^{-1})	K_d (mL g^{-1})	K	C_f (mg L^{-1})	K_d (mL g^{-1})	K	
Nd(III)	34.832	435.461		46.564	73.789		
La(III)	45.441	100.325	0.230	46.784	68.732	0.931	0.247
Gd(III)	45.853	90.441	0.208	46.824	67.835	0.919	0.226
Dy(III)	45.812	91.417	0.210	47.225	58.772	0.796	0.264
Tb(III)	45.652	95.232	0.219	46.921	65.621	0.889	0.246

Table 5 Comparison of REEs adsorption capacity for different Sorbents

Sorbents	Cation	PH	Adsorption capacity (mg g^{-1})	Selectivity	References
IMCFs	Nd(III)	4.0	22.61	High	This study
Dual-template docking oriented ionic imprinted mesoporous films	Nd(III)	3.0	34.98	High	Zheng et al. (2017)
Imprinted mesoporous silica materials	Dy(III)	2.0	22.33	High	Zheng et al. (2016)
Yeast cells	Nd(III)	1.5	10-12	–	Vlachou et al. (2009)
Ionic imprinted polymer particles	Nd(III)	7.5	33	High	Krishna et al. (2005)
Phosphonic acid functionalized silica microspheres	Nd(III)	2.8	45	–	Melnyk et al. (2012)
Molecularly imprinted polymers	Nd(III)	5.5	14.6	High	Dolak et al. (2015)

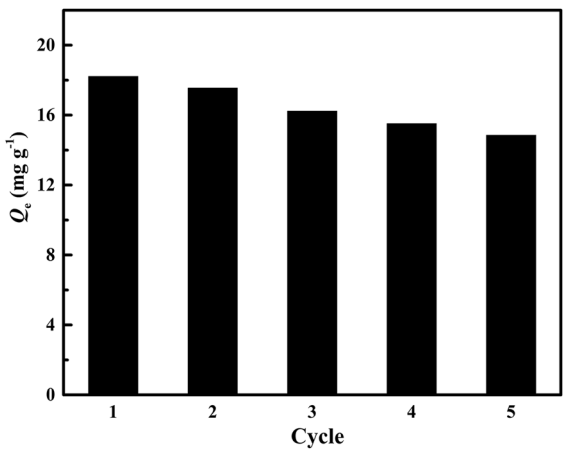

Fig. 8 Reusability of IMCFs over 5 cycles

adsorption performance of IMCFs decreased to 81.55% of the initial adsorption capacity. In addition, there is no significant change between pristine IMCFs and regenerative IMCFs by XRD in Fig. S3. This can be attributed to surface ionic imprinting. Strong mechanical properties of CNCs and surface ionic imprinting provide stable and selective imprinted sites, greatly improve stripping and adsorption efficiency. Repeatability tests indicate IMCFs are high stable and reliable adsorbents in practical applications.

Conclusion

Imprinted mesoporous cellulose films were prepared via a green, one-step reaction, and employed for adsorption and separation of Nd(III) from end-of-life magnets under acidic system. CNCs containing rich functional groups on the surface were selected as mesoporous matrix, the coexistence of no need additional functional monomer, and mesoporous channel is the advantage of this strategy, compared

with other imprinting techniques. To better simulate the harsh adsorption environment and to more clearly compare the differences between IMCFs and NIMCFs, we adjusted pH of stock solutions to 4. The maximum adsorption capacity of IMCFs was 23.03 mg g^{-1}, more in accordance with the Langmuir model, proving IMCFs and NIMCFs implements monolayer adsorption. The distribution coefficient of Nd(III) reached 435.46 mL g^{-1}, which indicates IMCFs possess high adsorption efficiency and adsorption selectivity. Reusability tests proved IMCFs are feasible and stable for industrial application, which may provide an alternative for recovery of REEs.

Acknowledgments This work was financially supported by National Natural Science Foundation of China (Nos. 21576120, 21446015, 21507045, 21876015, 21808018, U1407123, U1507115 and U1507118) and Natural Science Foundation of Jiangsu Province (Nos. BK20140534, BK20140580, BK20151350 and BK20131223). Postgraduate Research & Practice Innovation Program of Jiangsu Province (SJCX18_0958).

References

Bian Y-Y, Guo S-Q, Xu Y-L, Tang K, Lu X-G, Ding W-Z (2015) Recovery of rare earth elements from permanent magnet scraps by pyrometallurgical process. Rare Met. https://doi.org/10.1007/s12598-015-0554-x

Chen Y, Wang H, Pei Y, Ren J, Wang J (2015) pH-controlled selective separation of neodymium (III) and samarium (III) from transition metals with carboxyl-functionalized ionic liquids. ACS Sustain Chem Eng 3:3167–3174. https://doi.org/10.1021/acssuschemeng.5b00742

Dai X, Wu S, Li S (2018) Progress on electrochemical sensors for the determination of heavy metal ions from contaminated water. J Chin Adv Mater Soc 6:91–111. https://doi.org/10.1080/22243682.2018.1425904

Dolak İ, Keçili R, Hür D, Ersöz A, Say R (2015) Ion-imprinted polymers for selective recognition of neodymium(III) in environmental samples. Ind Eng Chem Res 54:5328–5335. https://doi.org/10.1021/acs.iecr.5b00212

Du E, Li J, Zhou S, Zheng L, Fan X (2018) Transformation of naproxen during the chlorination process: products identification and quantum chemistry validation. Chemosphere 211:1007–1017

Dufresne A (2017) Cellulose nanomaterial reinforced polymer nanocomposites. Curr Opin Colloid Interface Sci 29:1–8

eFlorek J, Chalifour F, Bilodeau F, Lariviere D, Kleitz F (2014) Nanostructured hybrid materials for the selective recovery and enrichment of rare earth elements. Adv Funct Mater 24:2668–2676

Fröhlich P, Lorenz T, Martin G, Brett B, Bertau M (2017) Valuable Metals—recovery processes, current trends and recycling strategies. Angew Chem Int Ed 56:2544–2580. https://doi.org/10.1002/anie.201605417

Fu J, Chen L, Li J, Zhang Z (2015) Current status and challenges of ion imprinting. J Mater Chem A 3:13598–13627

Gao Y, Jin Z (2018) Iridescent chiral nematic cellulose nanocrystal/polyvinylpyrrolidone nanocomposite films for distinguishing similar organic solvents. ACS Sustain Chem Eng 6:6192–6202

Johannesson KH et al (2017) Rare earth element behavior during groundwater-seawater mixing along the Kona Coast of Hawaii. Geochim Cosmochim Acta 198:229–258. https://doi.org/10.1016/j.gca.2016.11.009

Krishna PG, Gladis JM, Rao TP, Naidu GR (2005) Selective recognition of neodymium(III) using ion imprinted polymer particles. J Mol Recognit 18:109–116

Lagerwall JP, Schütz C, Salajkova M, Noh J, Park JH, Scalia G, Bergström L (2014) Cellulose nanocrystal-based materials: from liquid crystal self-assembly and glass formation to multifunctional thin films. NPG Asia Mater 6:e80

Langmuir I (1916) The constitution and fundamental properties of solids and liquids. Part I. Solids. J Am Chem Soc 38:2221–2295. https://doi.org/10.1021/ja02268a002

Li B, Zhang Y, Wu C, Guo B, Luo Z (2018) Fabrication of mechanically tough and self-recoverable nanocomposite hydrogels from polyacrylamide grafted cellulose nanocrystal and poly (acrylic acid). Carbohydr Polym 198:1–8

Liu Y et al (2015) Thermal-responsive ion-imprinted polymer based on magnetic mesoporous silica SBA-15 for selective removal of Sr(II) from aqueous solution. Colloid Polym Sci 293:109–123. https://doi.org/10.1007/s00396-014-3393-7

Melnyk IV, Goncharyk VP, Kozhara LI, Yurchenko GR, Matkovsky AK, Zub YL, Alonso B (2012) Sorption properties of porous spray-dried microspheres functionalized by phosphonic acid groups. Microporous Mesoporous Mater 153:171–177. https://doi.org/10.1016/j.micromeso.2011.12.027

Moloney MP, Causse J, Loubat C, Grandjean A (2014) Sodium "Activation" of silano-phosphonate modified mesoporous TiO_2 leading to improved rare-earth element extraction. Eur J Inorg Chem 2014:2268–2277

Moriwaki H et al (2016) Application of freeze-dried powders of genetically-engineered microbial strains as adsorbents for rare earth metal ions 8:26524–26531

Pan J, Chen W, Ma Y, Pan G (2018) Molecularly imprinted polymers as receptor mimics for selective cell recognition. Chem Soc Rev 47:5574–5587

Patra S, Roy E, Madhuri R, Sharma PK (2017) Removal and recycling of precious rare earth element from wastewater samples using imprinted magnetic ordered mesoporous carbon. ACS Sustain Chem Eng 5:6910–6923. https://doi.org/10.1021/acssuschemeng.7b01124

Royen H, Fortkamp U (2016) Rare earth elements-purification, separation and recycling. IVL Swedish Environmental Research Institute, Stockholm, Sweden

Service RF (2005) How far can we push chemical self-assembly? Science 309:95. https://doi.org/10.1126/science.309.5731.95

Sprecher B, Kleijn R, Kramer GJ (2014) Recycling potential of neodymium: the case of computer hard disk drives.

Environ Sci Technol 48:9506–9513. https://doi.org/10.1021/es501572z

Sun Y, Shao D, Chen C, Yang S, Wang X (2013) Highly efficient enrichment of radionuclides on graphene oxide-supported polyaniline. Environ Sci Technol 47:9904–9910

Swain B (2017) Recovery and recycling of lithium: a review. Sep Purif Technol 172:388–403

Terpstra AS, Arnett LP, Manning AP, Michal CA, Hamad WY, MacLachlan MJ (2018) Iridescent chiral nematic mesoporous organosilicas with alkylene spacers. Adv Opt Mater 6:1800163

Tunsu C, Petranikova M, Ekberg C, Retegan T (2016) A hydrometallurgical process for the recovery of rare earth elements from fluorescent lamp waste fractions. Sep Purif Technol 161:172–186. https://doi.org/10.1016/j.seppur.2016.01.048

Vlachou A, Symeopoulos B, Koutinas A (2009) A comparative study of neodymium sorption by yeast cells. Radiochim Acta Int j Chem Aspects Nucl Sci Technol 97:437–441

Voisin H, Bergström L, Liu P, Mathew A (2017) Nanocellulose-based materials for water purification. Nanomaterials 7:57

Wang J, Han Y, Li J, Wei J (2017) Selective adsorption of thiocyanate anions using straw supported ion imprinted polymer prepared by surface imprinting technique combined with RAFT polymerization. Sep Purif Technol 177:62–70. https://doi.org/10.1016/j.seppur.2016.12.038

Wei X, Xu G, Gong C, Qin F, Gong X, Li C (2018) Fabrication and evaluation of sulfanilamide-imprinted composite sensors by developing a custom-tailored strategy. Sens Actuators B Chem 255:2697–2703

Won SW, Kwak IS, Mao J, Yun Y-S (2015) Biosorption–incineration–leaching–smelting sequential process for Ru recovery from Ru-bearing acetic acid waste solution. Ind Eng Chem Res 54:7148–7153. https://doi.org/10.1021/acs.iecr.5b01111

Xie F, Zhang TA, Dreisinger D, Doyle F (2014) A critical review on solvent extraction of rare earths from aqueous solutions. Miner Eng 56:10–28. https://doi.org/10.1016/j.mineng.2013.10.021

Xue J, Song F, Yin X-W, Zhang Z-L, Liu Y, Wang X-L, Wang Y-Z (2017) Cellulose nanocrystal-templated synthesis of mesoporous TiO_2 with dominantly exposed (001) facets for efficient catalysis. ACS Sustain Chem Eng 5:3721–3725

Yao K, Meng Q, Bulone V, Zhou Q (2017) Flexible and responsive chiral nematic cellulose nanocrystal/poly (ethylene glycol) composite films with uniform and tunable structural color. Adv Mater 29:1701323. https://doi.org/10.1002/adma.201701323

Yoon H-S, Kim C-J, Jeon S, Ilhwan P, Yoo K, Jha M, Chung KW (2015) The effect of grinding and roasting conditions on the selective leaching of Nd and Dy from NdFeB Magnet Scraps. Metals 5:1306–1314. https://doi.org/10.3390/met5031306

Zhao Y, Yu RL, Hu GR, Lin XH, Liu XR (2017) Characteristics and environmental significance of rare earth elements in PM2.5 of Nanchang, China. J Rare Earths 35:98–106. https://doi.org/10.1016/s1002-0721(16)60179-5

Zheng X, Liu E, Zhang F, Yan Y, Pan J (2016) Efficient adsorption and separation of dysprosium from NdFeB magnets in an acidic system by ion imprinted mesoporous silica sealed in a dialysis bag. Green Chem 18:5031–5040

Zheng X, Zhang F, Liu E, Xu X, Yan Y (2017) Efficient recovery of neodymium in acidic system by free-standing dual-template docking oriented ionic imprinted mesoporous films. ACS Appl Mater Interfaces 9:730–739. https://doi.org/10.1021/acsami.6b13049

Zheng X, Zhang Y, Zhang F, Li Z, Yan Y (2018) Dual-template docking oriented ionic imprinted bilayer mesoporous films with efficient recovery of neodymium and dysprosium. J Hazard Mater 353:496–504. https://doi.org/10.1016/j.jhazmat.2018.04.022

Zheng X, Wang Y, Qiu F, Li Z, Yan Y (2019a) Dual-functional mesoporous films templated by cellulose nanocrystals for the selective adsorption of lithium and rubidium. J Chem Eng Data 64:926–933

Zheng X, Zhang Y, Bian T, Zhang Y, Zhang F, Yan Y (2019b) Selective extraction of gadolinium using free-standing imprinted mesoporous carboxymethyl chitosan films with high capacity. Cellulose 26:1209–1219